Tackling Modern Sailing Challenges with a CFD-based Dynamic VPP

Pierre Robin, Alban Leroyer, David de Prémorel, Jeroen Wackers

Journal of Sailing Technology 2024, volume 9, issue 1, pp. 1-17.
The Society of Naval Architects and Marine Engineers.

Tackling Modern Sailing Challenges with a CFD-based Dynamic VPP

Pierre Robin
LHEEA Lab - Centrale Nantes/CNRS - Finot-Conq, France, pierre.robin@ec-nantes.fr.

Alban Leroyer
LHEEA Lab - Centrale Nantes/CNRS, France.

David de Prémorel
Finot-Conq Architectes Navals, France.

Jeroen Wackers
LHEEA Lab - Centrale Nantes/CNRS, France.

Manuscript received September 05, 2023; revision received November 19, 2023; accepted January 2, 2024.

Abstract. A dynamic Velocity Prediction Program (VPP) integrated in a Computational Fluid Dynamics (CFD) code is described. Aerodynamic forces are obtained either through empirical coefficients or interpolated from aerodynamics matrices. These aerodynamic forces are then input to the hydrodynamics CFD solver, which solves both the flow and the motions of the boat, resulting in a closely coupled VPP. For a given True Wind Angle and True Wind Speed a sail power parameter is optimised to obtain the best possible boat speed within heel angle constraints. This approach allows naval architects to swiftly and precisely compare several yacht designs in real sailing configurations using only a few CFD computations. Several advanced features recently added to this program are covered in this paper including convergence criteria, automatic grid refinement, foil fluid-structure interaction, multiple aerodynamics models and rudder control. Results obtained from our CFD VPP on a 40-feet fast-cruising yacht demonstrates promising agreement with other existing VPP polars, affirming the accuracy and reliability of our approach. The CFD VPP presented was also successfully applied to an IMOCA, a 60-feet racing yacht.

Keywords: CFD; VPP; sailing; hydrofoil; optimisation; FSI.

NOMENCLATURE

$C_{L_{\text{sailset}}}, C_{L_{\max}}$	Sailset's Aerodynamic Lift Coefficient, Sailset's Maximum Aerodynamic Lift Coefficient [-]
C_{sail}, C_{Fx}	Aerodynamic coefficient (Force or Torque), Surge aerodynamic coefficient [-]
e	Bearing angle error [°]
F_x, F_y, F_z	Aerodynamic Force along x-axis, y-axis, z-axis [N]
K_d, K_i, K_p	Derivative, Integral and Proportional Gains [-]
M_x, M_y, M_z	Aerodynamic Torque around x-axis, y-axis, z-axis [N.m]
$M_{x,\text{hydro}}$	Yacht's Righting Moment [N.m]
P_{ow}	Sail Power Parameter [-]
Re	Reynolds Number [-]
S	Sail Surface [m^2]
t_{cs}	Duration of Convergence Data Collection [s]
t_{start}	Start Time for Convergence [s]
t_{laps}	Duration between Successive Convergence Tests [s]
V_B	Yacht's Speed [kn]
$V_{B,\text{init}}$	Initial Yacht's Speed [kn]

V_t	True Wind Speed [kn]
V_a	Apparent Wind Speed [kn]
$y^+, y^+_{\max}, y^+_{\min}$	Wall distance, Maximal value of wall distance, Minimal value of wall distance [-]
α_1	Average of the Absolute Value of the Deviation from the Mean Value [-]
α_2	Maximal Absolute Value of the Deviations from the Mean Value [-]
$\alpha_{1,\mathrm{ref}}, \alpha_{2,\mathrm{ref}}$	Respective thresholds of α_1 and α_2 [-]
β_a	Apparent Wind Angle [°]
β_t	True Wind Angle [°]
δ	Rudder angle [°]
θ	Yacht's Pitch Angle [°]
ϕ	Yacht's Heel angle [°]
ρ	Fluid Density [kg.m^{-3}]
φ	Radial-Basis Function [-]
ω	Traveller position [m]
AGR	Adaptive Grid Refinement
AWA	Apparent Wind Angle
AWS	Apparent Wind Speed
CFD	Computational Fluid Dynamics
CPU	Central Processing Unit
DoF	Degree of Freedom
FSI	Fluid-Structure Interaction
IMOCA	International Monohull Open Class Association
MS-FCH	Multi-Surface and Flux-Component Hessian
TWA	True Wind Angle
TWS	True Wind Speed
VPP	Velocity Prediction Program

1 INTRODUCTION

Velocity Prediction Programs (VPP) have been used in the design of modern sailing ships for a few decades. For naval architects, these tools allow to assess and compare the performance of several yacht designs and eventually identify the best one, and as computer technology improves so do VPP codes. Classic static VPPs compute the equilibrium of the forces applied to the yacht and most rely on an interpolation performed in a matrix of the hydrodynamic forces.

This matrix, previously obtained with towing tank trials, is now computed using CFD simulations in 80 to 200 configurations (with different combinations of pitch, trim, draft, heel, speed, etc.). Even with the relentless progresses made in this field, such calculations are very expensive in CPU-time. Moreover, with such a process, any change in the hull design means that a new matrix should be computed, since the hydrodynamic forces applied on the yacht are likely to be different. Thus, traditional VPPs are somewhat impractical for hull-shape optimisation. Additionally, the CFD is performed on an isolated hull, so the interactions with the appendages are approximate at best, if not neglected entirely. Furthermore, although ship performance in waves will be a major challenge in coming years for offshore sailing, predicting motion in a sea state with a VPP remains difficult: it can only be approximated using successive steady-state force inputs.

For these reasons, we developed a dynamic VPP in which the forces from an analytic or matrix lookup aerodynamic model are directly applied to the boat during the CFD computation, while the hydrodynamics flow solver handles the hydrodynamic forces and the motions of the yacht. This approach results in dynamic changes in all degrees of freedom (DoF), such as trim, sinkage, heel, etc, leading to a coupling between aerodynamic and hydrodynamic effects. Roux et al. (2008) already performed

5-DoF simulations using a coupling between a CFD code solving hydrodynamics and a potential-flow code computing aerodynamic forces for an AC90 yacht, proving the feasability of an aerodynamic force input to the FINE/Marine solver. Later, Böhm (2014), Lindstrand Levin and Larsson (2017) and Persson et al. (2021) presented VPPs using CFD solvers to compute hydrodynamic forces and body motions, with aerodynamics relying on analytical models. All three VPP programs were successfully applied to a range of boats including a Laser dinghy (Lindstrand Levin and Larsson, 2017), an AC90 yacht (Böhm, 2014), and the Sailing Yacht Research Foundation (SYRF) yacht (Persson et al., 2021). For both the AC90 and the SYRF yacht, polars were obtained within acceptable delays for a complete (0-180°) range of True Wind Angle (TWA) and for one or several True Wind Speeds (TWS). However, it is important to note that none of these works were explicitly developed with a focus on accommodating foil-equipped yachts or addressing ship-in-wave performance. Their primary objective centered on finding equilibrium states, and optimise yacht speed, similar to the approach of a conventional static VPP.

The main innovation of our work is to create a high-fidelity dynamic VPP whose aim is not to provide a complete polar for the studied design, but to compare different designs in key wind conditions all along the design process. Our VPP uses a similar procedure as the works of Böhm (2014) and Persson et al. (2021), but is also intended to be used dynamically, to simulate a yacht in waves for instance. Since our VPP is tailored for intensive use by the naval architect company that developed it, and for the simulation of modern foiling sailing yachts, especially IMOCAs, it uses modern techniques that have proven their usefulness when simulating a sailing ship. Indeed, since our VPP program is embedded in the commercial CFD suite FINE/Marine, several advanced features already in the software can be used, such as overset grids, quasi-static body motions, adaptive grid refinement, and the modal approach for fluid-structure interactions.

In addition to this, other features more tailored to our use have been developed, including a PID-controlled rudder, a sock-mesh approach for foils and VPP-tailored convergence control. Since time-accurate simulation is still under development, this paper will mainly focus on the computation of steady-state solutions used to optimise the yacht's speed. However, as a "roadmap" for the future, it also presents some of the features under development for ship-in-waves simulations.

The development of this new tool reflects Finot-Conq's strategy to incorporate more high-fidelity simulations in their design process, while limiting the associated CPU costs. The VPP covered in this paper has been used for Finot-Conq's two new IMOCAs (Paprec-Arkéa and For People), launched in early 2023 with the goal of winning the Vendée Globe in 2024-2025.

Section 2 provides details of the VPP algorithm, while section 3 covers the aerodynamic modules. The hydrodynamic solver is discussed in section 4. Finally, section 5 presents results obtained using the VPP.

2 VPP ALGORITHM

Our dynamic CFD-based VPP, is integrated in the commercial CFD software FINE/Marine (Queutey and Visonneau, 2007; Wackers et al., 2011). It allows naval architects to optimise boat speed as a function of the sail trim (represented by a sail power parameter P_{ow}, see Section 3) in a single 5 or 6 DoF computation.

The general process of the VPP is described in Fig. 1. The VPP is a module added to FINE/Marine, thus its use requires first to set up a classical FINE/Marine computation. Placing the yacht in a configuration close to its final position (in terms of cardan angles and displacement) will help the simulation to converge and reduce CPU-time. Additionally, the VPP module requires the user to provide a True Wind Angle (TWA) β_t, a True Wind Speed (TWS) V_t and some of the yacht's main characteristics (length over all, freeboard height, air draft, etc.).

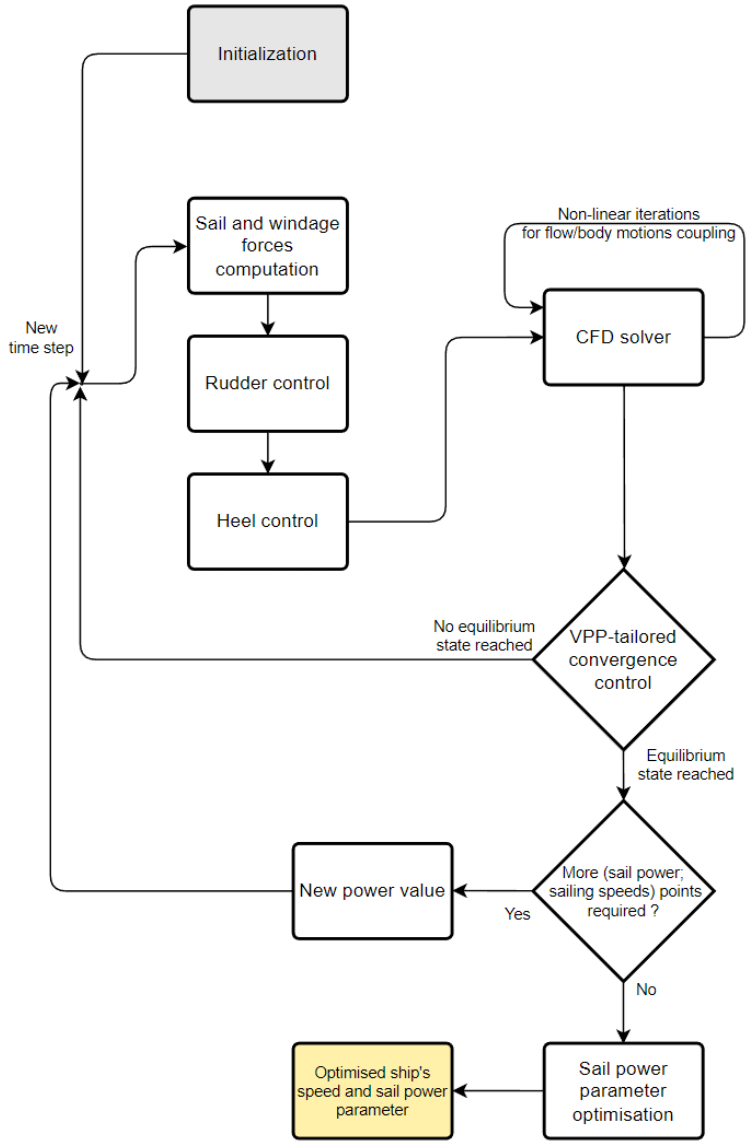

Figure 1. VPP code general process.

Once this data is read and FINE/Marine has started, the VPP code updates sail forces at each time step (covered in Section 3), adjusts the rudder angle (Section 2.1), and keeps the heel of the yacht within user-specified bounds (Section 2.3). The resulting forces and moments are then input to the flow solver ISIS-CFD, which solves the flow and the motions of the yacht. During the simulation, the VPP checks if an equilibrium state is reached using a specific set of convergence criteria (Section 2.2). If these criteria are satisfied, a new value for the sail power parameter P_{ow} is chosen by the optimisation algorithm and used in a new stage of the same computation. At the end of the computation, several equilibrium states have been found (and thus several V_B-P_{ow} doublets), and the VPP outputs an optimised boat speed V_B and sail power parameter P_{ow} for the yacht's geometry and the doublet (V_t, β_t) provided.

2.1 Rudder Models

For course control, an analytical rudder model is employed to balance the Mz moment arising from the forces acting upon the vessel. For this model, the user has to supply a boat geometry without a rudder, as well as the requisite rudder polars. During the simulation, these polars are used to compute the rudder angle from the targeted Mz moment. All rudder forces are then assessed at the computed angle and transmitted to the flow solver.

However, to improve the accuracy of the boat's behavior, and in the scope of carrying out future ship-in-waves simulations, a second approach using a CFD-modelled rudder with a PID controller is being developed. For this approach, the rudder geometry needs to be included and is placed in an overset domain (see section 4.1). The rudder angle $\delta(t)$ is controlled using, as error e, the difference between the yacht's course angle and a given target bearing. The rudder angle is updated with a given period T using the following law:

$$\delta(t) = K_p\, e(t) + K_i \int_{t-T}^{t} e(t)\,\mathrm{d}t + K_d\, \frac{\mathrm{d}e(t)}{\mathrm{d}t}. \tag{1}$$

In addition to this PID-controller, a simplified model of an autopilot's actuator has been implemented with realistic angular speed limitations. This method is still a work in progress, as only linear integration and derivation schemes are implemented and the gains K_p, K_i, K_d are, for the moment, determined by trial-and-error and will require fine-tuning using dedicated methodologies.

2.2 Convergence Criteria

To test if the yacht has reached an equilibrium state, specific convergence criteria have been implemented. Indeed, yachts equipped with foils can induce small-scale unsteadiness in the computation, thus requiring to make sure that key physical quantites undergo limited changes around a converged value. To do so, the user has to specify:

- Which physical values (forces, moments, motion quantities) will be studied for convergence,
- After how much simulation time the convergence check is first carried out (t_{start}),
- The amount of time between two convergence tests (t_{laps}),
- The duration (in seconds) of data collected to form a convergence sample t_{cs},
- For every physical value, two thresholds for the data: $\alpha_{1,\mathrm{ref}}$ and $\alpha_{2,\mathrm{ref}}$.

Indeed, for every physical value studied and given that enough time has passed, two indicators are computed over the last t_{cs} seconds of the simulation: the average of the absolute value of the deviation from the mean value α_1, whose expression for a quantity x is:

$$\alpha_1 = \frac{1}{t_{\mathrm{cs}}} \sum_{t_{\mathrm{cs}}} |x - \overline{x}|, \tag{2}$$

with :

$$\overline{x} = \sum_{t_{\mathrm{cs}}} x \quad \text{if } t > t_{\mathrm{start}}. \tag{3}$$

But also the maximal absolute value of the deviations from the mean value α_2, whose expression for a quantity x is:

$$\alpha_2 = \max_{t_{\mathrm{cs}}} |x - \overline{x}|. \tag{4}$$

If for every physical value studied, α_1 and α_2 are inferior to their respective thresholds $\alpha_{1,\mathrm{ref}}$ and $\alpha_{2,\mathrm{ref}}$, an equilibrium state is considered to be reached. A typical value for t_{cs} is 1.5 times the hull length divided by its speed, while $\alpha_{1,\mathrm{ref}}$ and $\alpha_{2,\mathrm{ref}}$ are usually comprised between 0.01 and 0.05. The workflow of the method is described in Fig. 2.

2.3 Sail Power Parameter Optimisation

To find the optimum yacht's speed at a given operating point, the sail power parameter P_{ow}, that represents the crew trimming the sails, is optimised. The way this parameter affects the sail forces will be covered in Section 3.

In a single VPP computation, several equilibrium states are reached, each one being associated with an intermediate calculation using a different value of P_{ow}. A minimum of 3 intermediate calculations

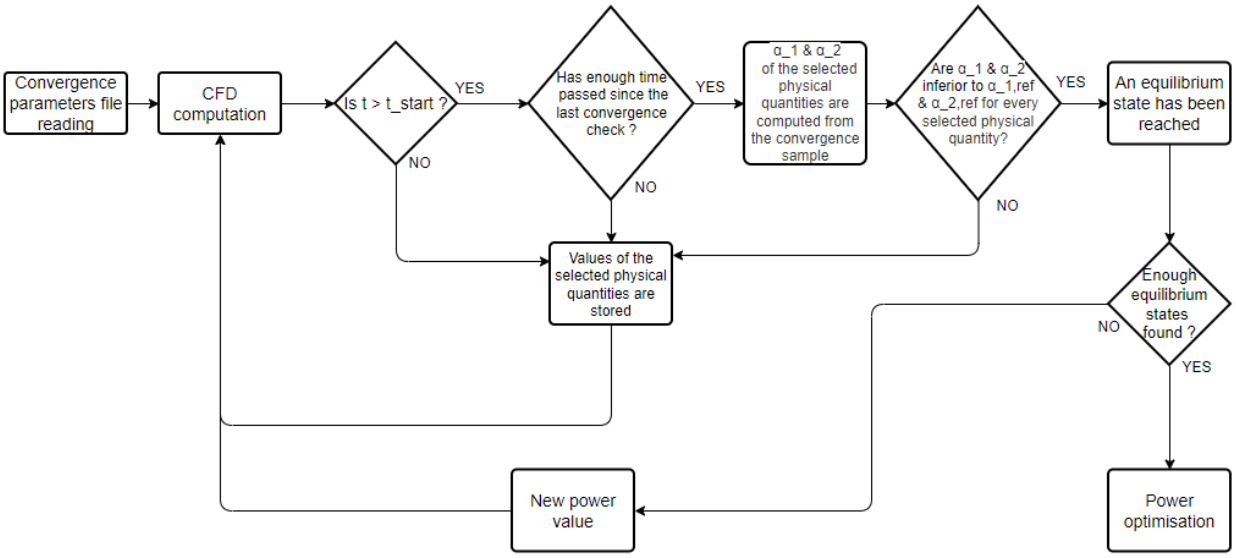

Figure 2. VPP convergence method diagram.

is required to calculate an optimum value of P_{ow}, but more can be performed if desired, to refine the optimum values obtained. During each intermediate calculation, the sail power parameter P_{ow} may be adjusted if needed to keep the yacht's heel angle ϕ between the boundaries specified by user.

The first intermediate computation is initiated with the parameter's maximum value. Once it is considered converged, P_{ow} is set to its minimum value. Once the second intermediate computation has converged, a third one starts with the mean value of the two previously used. Then the VPP code finds an optimal value for P_{ow} using parabolic optimisation, based on the first three iterations. If more points are required by the user, another computation starts with P_{ow} set at the computed optimum. At the end of this computation, a new parabolic optimisation is performed and a new optimum of P_{ow} is found.

Previous work at Finot-Conq attempted to perform sail power parameter optimisation using other methods, but parabolic optimisation was chosen as the most CPU-efficient. It has also proven to be sufficient as the relationship between V_B and P_{ow} is correctly captured by a parabola. For the same reason, multi-criterion optimisation using reefing along with sail power was discarded. Indeed, it is more efficient and more realistic to perform separate VPP runs for different sail plans, due to the discontinuous nature of reefing on a real yacht.

An example of results for a 40-feet fast cruiser is presented in Tab. 1 and Fig. 3. The maximal speed of the yacht is not reached for the maximum value of sail power parameter, as a reduced heel allows the boat to sail faster. The 4th optimisation iteration eventually presented a limited interest here, since the difference in speed obtained at the end of the 4th iteration (0.8488) is really close to the optimum computed at the end of the 3rd iteration (0.8471).

Table 1. Example of results of optimisation for a 40-feet fast cruiser (sail power range: 0.62 - 1).

Iteration	P_{ow} [-]	V_B [kn]	ϕ [°]
1	0.9343	6.45	-23.00
2	0.6200	6.14	-11.86
3	0.7772	6.47	-17.39
4	0.8471	6.53	-20.01
Optimum found	0.8488	6.53	not computed

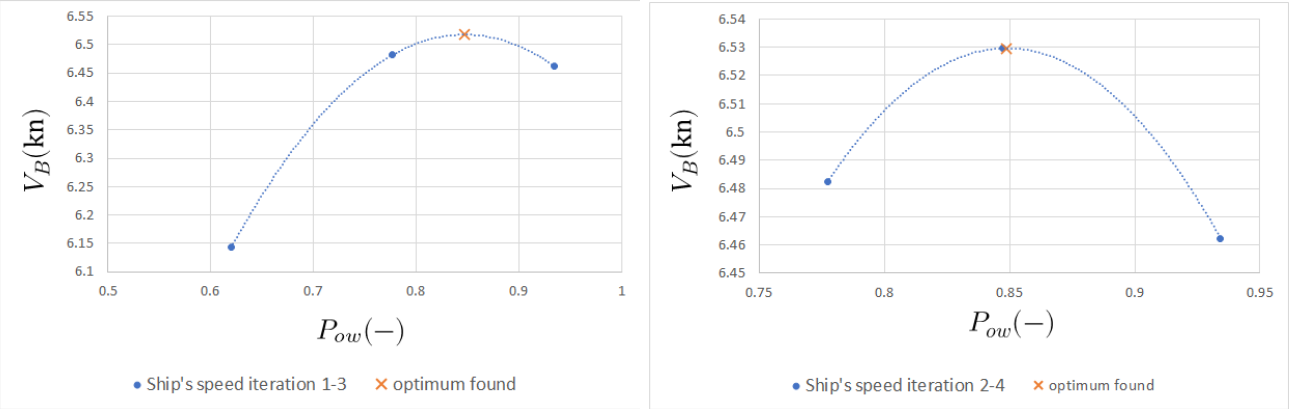

(a) Sail power parameter optimisation using points 1-3. **(b)** Sail power parameter optimisation using points 2-4.

Figure 3. Example of sail power parameter P_{ow} optimisation.

3 AERODYNAMIC LIBRARY

A pivotal aspect of the Velocity Prediction Program (VPP) code is the computation of aerodynamic forces. The VPP can employ analytical models for the determination of sail aerodynamics, or alternatively perform interpolation from a structured data matrix. The forces and moments exerted by the sails onto the vessel are assumed to depend on AWA β_a, AWS V_a, and the sail trim, which is characterized by the sail power parameter P_{ow}. When using the aerodynamic matrices, the heel angle ϕ is also taken into account. These aerodynamic forces are computed at each time step to accurately accommodate any change in these quantities.

3.1 Analytical Models

Aerodynamic forces and moments can be computed using the formulas and coefficients presented in the Offshore Racing Congress (ORC) VPP methodology (ORC, 2021). When using this method, the sail power parameter P_{ow} that will be optimised acts as the $flat$ parameter described in the ORC VPP aerodynamic model. It is applied linearly to the lift coefficient of the considered sail plan $C_{L_{\text{sailset}}}$:

$$C_{L_{\text{sailset}}} = P_{ow} C_{L_{\max}}, \tag{5}$$

with $C_{L_{\max}}$ the maximum lift coefficient of the sailset, derived from the sails' geometry and empirical sail aerodynamics coefficients.

P_{ow} also influences the sails' drag, but a detailed exposition of its mechanics would involve intricate equations beyond the scope of this paper. For further details, the reader is encouraged to refer to the ORC VPP documentation (ORC, 2021).

3.2 Interpolation from Aerodynamics Matrices

In addition to this analytical model, the VPP can use aerodynamics matrices obtained by external CFD computations, typically those made by the sailmakers. At each time step of the VPP calculation, an interpolation module based on cubic interpolations supplies the VPP code with aerodynamic coefficients C_{sail} based on this data (where C_{sail} stands for C_{Fx}, C_{Fy}, ... , C_{Mz}) . When using this approach, P_{ow} is also the parameter that captures the trim of the sails (through the sheet length) but it acts on the forces and moments only as one of the variables of the interpolation used to determine C_{sail}:

$$C_{\text{sail}} = f(P_{ow},\, \beta_a,\, \phi), \tag{6}$$

with C_{sail} the appropriate aerodynamic coefficient for the moment or force considered, and f a cubic interpolation function. With this approach, $P_{ow} = 0$ means the sails are trimmed to the lowest practi-

cally useful power. Contrary to the analytical models, it does not imply that the aerodynamic forces are zero.

Once the six aerodynamics coefficients are determined, the forces and moments are computed using the following formula:

$$F_{sail} = \frac{1}{2}\,\rho\,S\,C_{\text{sail}}\,V^2, \tag{7}$$

with F_{sail} the aerodynamic force or torque (F_x, F_y, ... M_z), ρ the air density, S the surface of the considered sail, and V the velocity of the flow at the sail's effort height (obtained from V_a).

Results for the surge coefficient C_{Fx} obtained using this interpolation method for a mainsail and jib aerodynamics matrix are presented in Fig. 4.

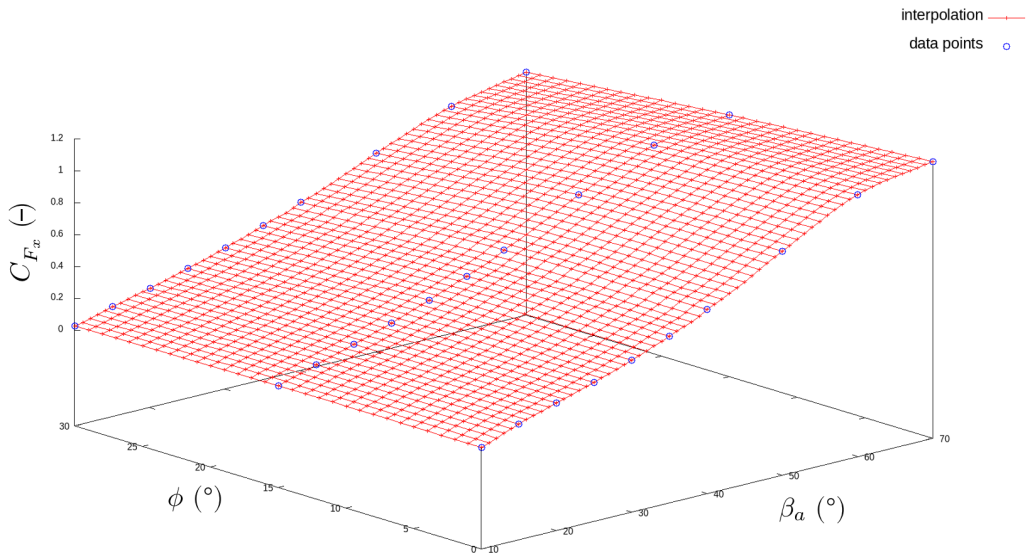

Figure 4. Surge coefficient C_{Fx}interpolation using cubic interpolations on AWA and heel. P_{ow} is fixed and equal to 1.

3.3 Windage

Windage forces acting on the different parts of the sailing boat (hull, mast, rigging, crew, etc.) are also computed using the ORC VPP methodology. In some sailmakers' aerodynamic matrices, these forces are already taken into account, thus no additional windage forces need to be computed.

4 HYDRODYNAMIC SOLVER

FINE/Marine is a marine-oriented computing suite, distributed by Cadence Design Systems (formerly Numeca International) and used by many naval architects for various hydrodynamics applications. The suite features an unstructured hexahedral mesher called Hexpress, as well as the flow solver ISIS-CFD. The latter is an incompressible unsteady Navier-Stokes equations solver with various Reynold-Averaged Navier Stokes (RANS) or RANS/Large Eddy Simulation hybrid turbulence models for multifluid flows which is developed by the METHRIC team of the LHEEA Laboratory.

The solver ISIS-CFD features a mixture-fluid formulation to model the water-air interface (Queutey and Visonneau, 2007; Wackers et al., 2011). The flow equations are discretised in a finite-volume framework, using pressure-velocity coupling obtained through implicit time integration with a Rhie & Chow SIMPLE-type method. The discretisation is face-based. While all unknown state variables are cell-centred, the systems of equations used in the implicit time stepping procedure are constructed face by face. This technique poses no specific requirements on the topology of the cells. Therefore, the grids can be completely unstructured, and cells with an arbitrary number of arbitrarily-shaped

faces are accepted. The limited AVLSMART scheme (Pržulj and Basara, 2001) is used for all convective fluxes, except for the volume fraction which uses the compressive BRICS scheme (Wackers et al., 2011). Diffusive terms are represented with central differences. The software suite has been extensively tested for different types of simulations. Examples of tests can be found in Deng et al., 2015 for cargo ships, and Prince and Claughton, 2016 for sailing yachts.

All calculations presented in this paper used RANS equations and the $k-\omega$ SST turbulence model with wall functions. The y+ of the first viscous layer is chosen for each computation, dependent on the Reynolds number of the yacht. Following FINE/Marine best practices, this choice is made as:

$$y^+ = \max\left(y^+_{\min}, \min\left(30 + \frac{270\,(Re - 10^6)}{10^9}, y^+_{\max}\right)\right), \tag{8}$$

with $y^+_{\max} = 300$, $y^+_{\min} = 50$ and Re the Reynolds Number. Undisturbed far field conditions are imposed on all lateral boundaries with prescribed pressure on the top and bottom of the domain.

4.1 Computing Yacht Motions

For 5 or 6-DoF VPP computations, a coupling between the flow, the external forces and yacht motions is necessary as the motion of the yacht modifies the flow, and as the flow applies forces on the yacht, modifying its kinematics.

Thus, ISIS-CFD uses non-linear iterations inside each single time step to solve both the Navier-Stokes equations and the yacht's dynamics at the same time and perform the coupling between flow and body motion (Leroyer and Visonneau, 2005). For every non-linear iteration the motions of the yacht are updated, the mesh is deformed accordingly and the flow is solved. Forces and moments applied on the yacht can then be computed using the newly obtained flow before a new non-linear iteration starts.

To handle large motions of bodies, ISIS-CFD relies on an overset method, with a finely meshed domain around the body overlapping a background domain and moving through it. These two domains are dynamically coupled using interpolation, either through a least squares approach or with a weighted distance scheme. The VPP optimisation algorithm changes the sail power parameter, thereby inducing major changes in the yacht's attitude, making the use of overset grids a must. When simulating an IMOCA and all its appendages in the VPP, up to 4 overset domains are used: the hull and the keel are included in the yacht overset domain (blue in Fig. 5) which also contains two rudder overset domains (in red), as well as the sock-mesh overset domain for the foil (in yellow).

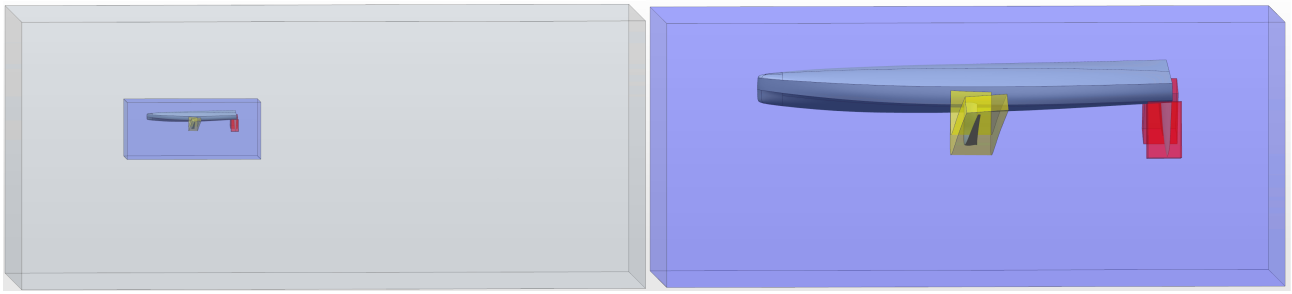

(a) Global view **(b)** Detailed view of the boat overset domain

Figure 5. Use of overset domains for a typical IMOCA VPP simulation.

4.2 Adaptive Grid Refinement and Sock-mesh Approach

FINE/Marine contains an adaptive grid refinement (AGR) algorithm, with several available criteria that allow the mesh to be automatically refined locally, during the computation (Wackers et al., 2017). Mesh adaptation enhances the capturing of flow details, either for waves, wake flows, or in boundary layers around bodies, especially around hydrofoil edges. This increases the accuracy of the forces for a given mesh size (Wackers et al., 2022).

When a good accuracy for the forces applied on bodies as well as a good understanding of the flow in the boundary layer is needed (which is typically the case in calculations involving hydrofoils) the Multi-Surface and Flux-Component Hessian (MS-FCH) criterion is preferred (Wackers et al., 2022). When using this AGR algorithm, the refinement criterion is based not only on the free-surface position but also on the Hessian of both pressure and velocity. Calculations using the MS-FCH criterion allow users to generate a coarse initial mesh on bodies, and to leave local mesh refinements to the AGR.

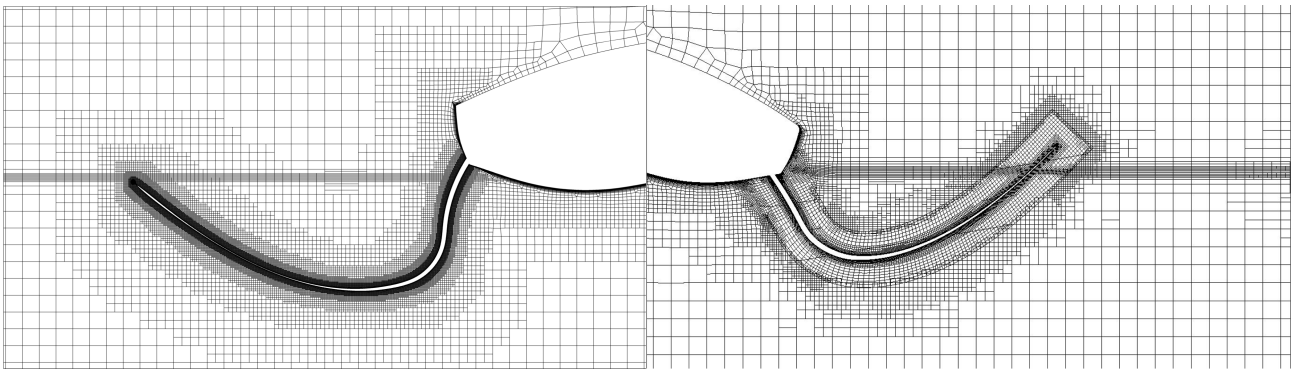

(a) Cut view of the mesh using a box-shaped domain **(b)** Cut view of the mesh using the sock-mesh approach

Figure 6. Comparison of meshing methods for IMOCA VPP simulation.

When simulating a boat equipped with foils, box-shaped domains are typically employed in Hexpress (FINE/Marine's mesh generator). For these, the cells are not aligned with the curved foil geometry, so the mesh generator creates many small cells of mediocre quality to capture the foil (see Fig. 6a). To tackle this issue, a good practice consists in using an initial curved overset domain whose shape follows the foil's shape (see Fig. 6b) in addition to the yacht's box-shaped domain, as this allows for better-quality initial meshes. Furthermore, the benefits of using the MS-FCH criterion are reinforced when using such a 'sock' initial mesh for the foil, since the initial mesh is of better quality and lighter, thus leading to better accuracy and CPU-time savings (Robin et al., 2022).

4.3 Fluid-structure Interaction

For IMOCA foils of roughly 6 meters length, the deflection at the tip can reach up to 1 meter in certain sailing conditions. These large deformations lead naval architects and engineers to take into account fluid-structure interactions for these appendages. Indeed, calculations and experience both show that fluid-structure interaction plays a major role in an IMOCA's foil's performance: its bending (mostly rotation of sections around the length-wise axis of the boat) modifies the ratio of vertical and lateral lift, while its torsion has a major influence on the lift distribution and therefore on the lift/drag ratio. The combination of both effects, depending upon the design of the foil, can have a stabilizing or a destabilizing influence on the yacht's behavior at sea. Accurate capturing of the foil deformations is therefore essential to correctly assess the performance of foiling or foil-assisted boats, both in a VPP-optimised steady equilibrium and in dynamic motion, for example in waves.

FINE/Marine handles fluid-structure interaction through a modal approach (Leroyer, 2021; Mouton et al., 2018). The first deformation eigenmodes of the structure are computed in an external finite element solver and input to the flow solver. During the computation, structural deformations are obtained by computing the temporal evolution of the amplitude of these selected eigenmodes through a modal equation solved internally. This approach allows for CPU-time savings, since this FSI approach does not need to interact directly with a structural solver during the flow resolution. In addition to this, using a third-part external FEA solver allows to account for any internal design, shape or material characteristics. The behaviour of the structure is computed using an internal module, and so is the rigid motion. The sock-mesh approach simplifies the handling of the mesh deformation around the foil as the domain is of limited size and its curves follow the foil's shape.

5 RESULTS

5.1 40-feet Fast Cruiser

Single Operating Point A VPP simulation has been carried out for a modern 40-feet fast cruiser, the Pogo 40, using the analytical aerodynamic model and the analytical rudder model covered previously. The parameters of the simulation are described in Tab. 2. In addition to Tab. 1 and Fig. 3 shown above, results for several physical quantities are presented in Fig. 7.

Table 2. Computation parameters for the 40-feet fast cruiser simulation.

V_t [kn]	β_t [°]	$V_{B,\text{init}}$ [kn]	Sail plan	P_{ow} range [-]
10	50	8	Mainsail + Jib	0.62-1

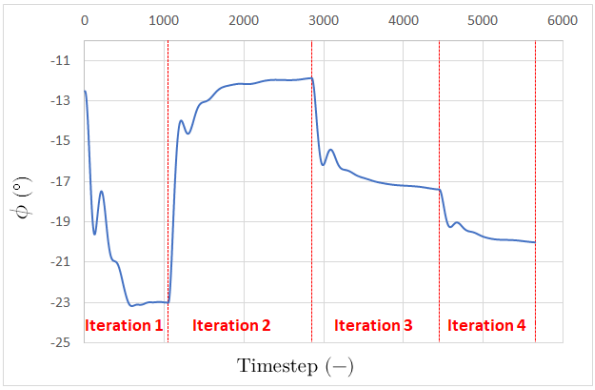

(a) Evolution of yacht's heel angle ϕ during the computation.

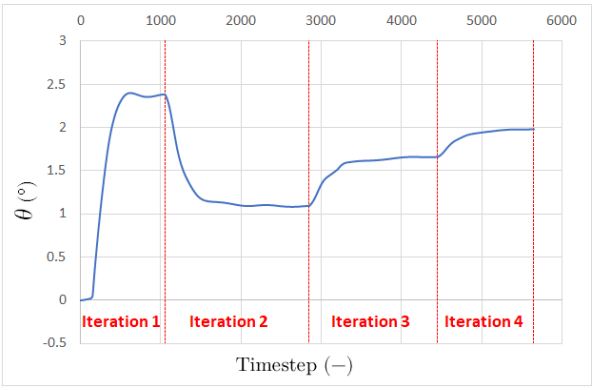

(b) Evolution of yacht's pitch angle θ during the computation.

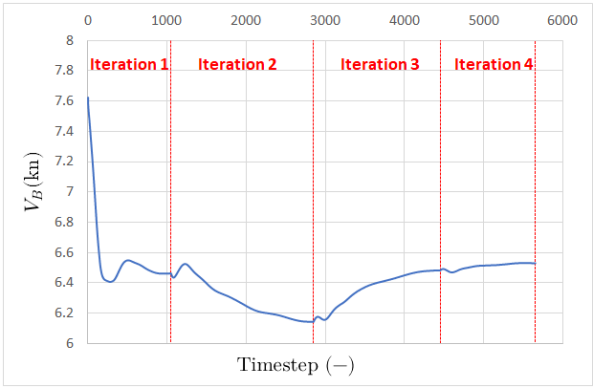

(c) Evolution of yacht's speed V_B during the computation.

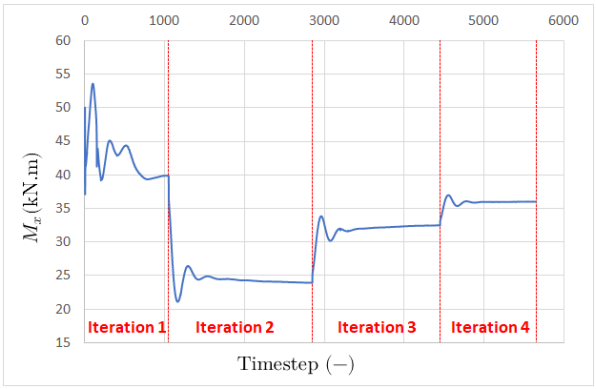

(d) Evolution of yacht's moment around x-axis $M_{x,\text{hydro}}$ during the computation.

Figure 7. Results for a 40 feet fast cruiser.

The impact of the change in sail parameter power can be clearly observed. When initially set to the maximum value (1.0), the sail power parameter eventually reaches a smaller value (0.9343) due to the maximal heeling being attained. Then the sail power parameter is set to its minimal value (0.62), the boat rights itself (Fig. 7a), but at the cost of a loss of speed (Fig. 7c). P_{ow} is then set to an intermediate value (0.7771), at which the boat sails faster than for the maximal sail power parameter value. Using these results, a first optimised point is computed, with a sail power parameter of 0.8470. When used as the input of a fourth iteration, it brings a better yacht's speed, and the final parabolic optimisation eventually finds an optimal sail power parameter value of 0.8488. In this upwind case, lowering the heel angle ϕ by reducing P_{ow} value results in a better sailing speed V_B than when $P_{ow} = 1$, due to an increased sail projected area.

Comparison of VPP polars A comparison is made between multiple operating points given by our CFD-based VPP and existing data provided by the ORC VPP. The polars obtained with the ORC VPP for the Pogo 40 are available in Waagmeest (2023). For our VPP, two different aerodynamic sail plan are used, corresponding to upwind and downwind sails. To reduce the computational time, only $V_t = 10$ kn has been considered.

Table 3. Computation parameters for the 40-feet fast cruiser polar.

V_t [kn]	β_t [°]	Upwind Sail Plan	Downwind Sail plan	P_{ow} range [-]
10	50-150	Mainsail + Jib	Mainsail + Spinnaker	0.62-1

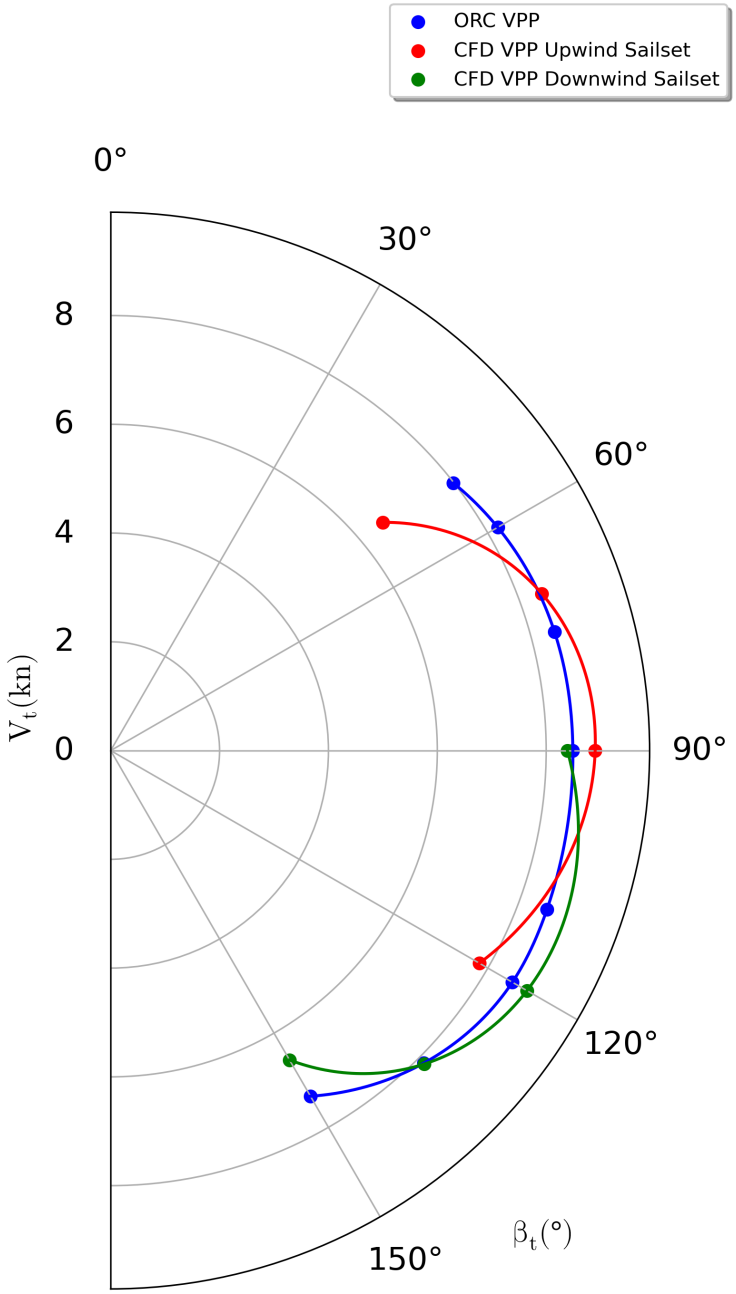

Figure 8. VPP polar comparisons.

Table 4. VPP Computation Results for the 40-feet Fast Cruiser, $\mathbf{V_t} = 10$ kn.

β_t [°]	V_B [kn]	ϕ [°]	optimal P_{ow} [-]
50	6.53	-20.0	0.85
70	8.43	-23.0	0.95
90	8.90	-16.5	1.00
120	7.82	-4.6	1.00
90	8.39	-23.0	0.89
120	8.83	-14.1	1.00
135	8.15	-6.2	1.00
150	6.57	-1.6	1.00

The results in Fig. 8 and Tab.4 show that our VPP agrees closely with the ORC data for moderate upwind and reaching angles. And while the ORC model does not explicitly show the position of the change in sailsets, this also appears to correspond well. For close-hauled and deep reaching conditions, our VPP predicts lower speeds than the ORC data. Based on sea trials and Finot-Conq experience, the yacht' speed for $\beta_t = 50°$ and for $\beta_t = 150°$ are overestimated by the ORC VPP ($V_B \approx 8$ kn), while the value given by the CFD-VPP seem more realistic.

5.2 IMOCA

The following calculations have been made during the design campaign of two IMOCAs for the Vendee Globe 2024. The simulated yacht has its canting keel and the leeward side foil. Interpolation in an aerodynamics matrix is used, as well as the analytical rudder model. Other parameters of the calculation are listed in Tab. 5.

Table 5. Computation parameters for the IMOCA 60' VPP simulation.

V_t [kn]	β_t [°]	$V_{B,\mathrm{init}}/V_B$ [-]	Sail Plan	P_{ow} range [-]
20	135	1	Mainsail + Code Zero	0-1

Results of the optimisation are presented in Tab. 6 and Fig. 10. For confidentiality reasons, the velocity has been normalized by the initial yacht speed $V_{B,\mathrm{init}}$. Also the forces and moments are normalised. The effect of the sail power parameter on various physical quantities can be observed in Fig. 9 and the effect on the yacht's attitude in Fig. 11. In this case, the maximum heel angle is set to 20° for external reasons. At the end of the first 3 iterations, it appears that the maximum speed is attained for the maximum power parameter, and no further iteration is necessary.

Table 6. Results of optimisation for an IMOCA.

Iteration	P_{ow} [-]	$V_B/V_{B,\mathrm{init}}$ [-]	ϕ [°]
1	0.9367	0.920	-19.99
2	0.0000	0.762	-10.14
3	0.4683	0.854	-14.23
Optimum found	0.9367	0.920	-19.99

For this particular computation, it was expected from previous computations done in a static VPP, that the maximum sailing speed would be obtained for the maximum value of P_{ow}. Hence, in order to compare the results given by our tool to those obtained with the static VPP, fine convergence criteria were applied to the first stage of the computation, where the VPP code looks for an equilibrium state associated with $P_{ow} = 1$. Coarser convergence criteria were applied during the following iterations, which have inferior sail power parameter values, to reduce CPU-time for this industrial project. However, based on (Fig. 9c, 9e), even with finer convergence criteria, the 3rd iteration would still produce a lower V_B than the first iteration (Fig. 10), which implies an optimal P_{ow} value that is identical to the result obtained with the coarse criteria. This confirms the results provided by the static VPP.

During the first iteration, the heel hits 20 degrees, as can be seen in Figure 9a. Consequently, as explained in paragraph 2.3, the sail power P_{ow} is diminished to keep the boat inside the heeling boundaries. This gives a final power of 0.93 for the first iteration. The sail power P_{ow} is limited by the heel angle only for the first iteration, and if the maximal heeling angle allowed was 25° instead of 20°, the sail power at the end of the first iteration might be 1.

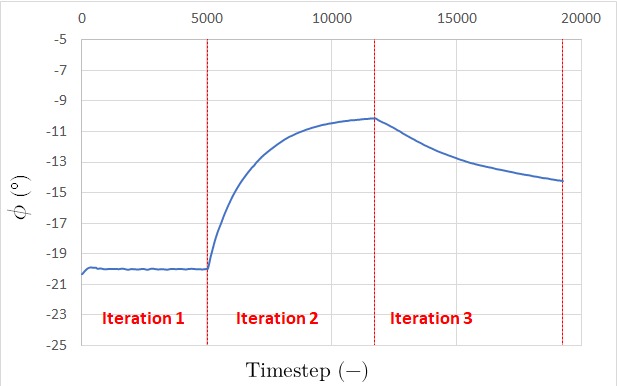

(a) Evolution of yacht's heel angle ϕ during the computation.

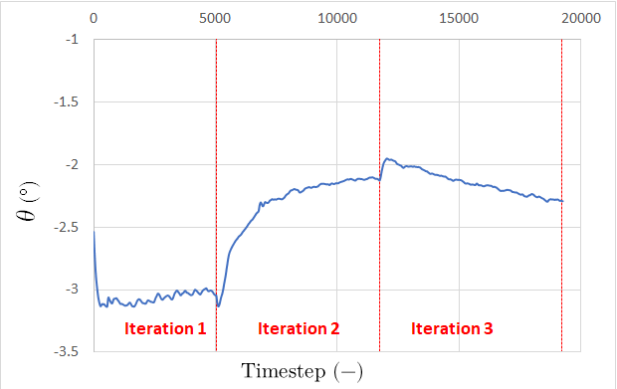

(b) Evolution of yacht's pitch angle θ during the computation.

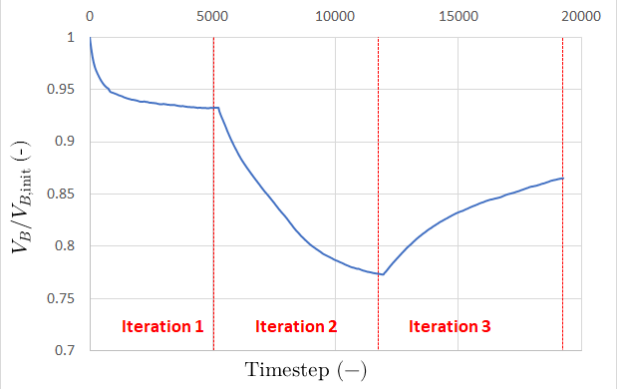

(c) Evolution of yacht's speed V_B during the computation.

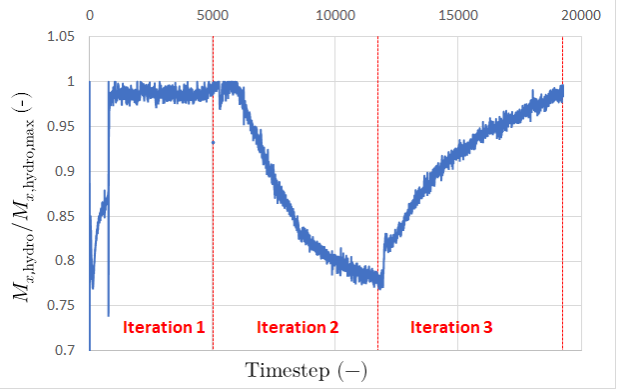

(d) Evolution of yacht's moment around x-axis $M_{x,\text{hydro}}$ during the computation.

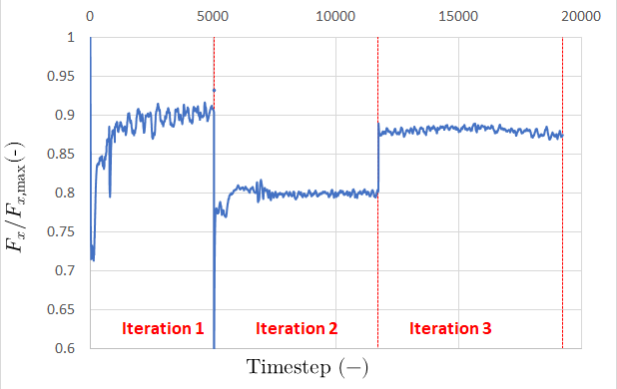

(e) Evolution of force along x-axis provided by the sails F_x during the computation.

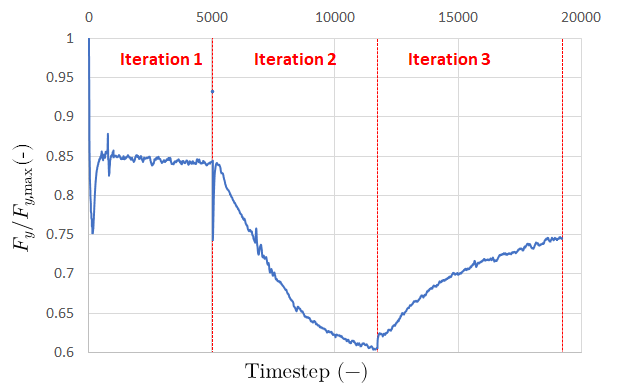

(f) Evolution of force along y-axis provided by the sails F_y during the computation.

Figure 9. Results for an IMOCA 60' VPP simulation.

The results in Fig. 11 highlight the link between the sails' power P_{ow} and the attitude of the boat. When P_{ow} is close to its maximal value (Fig. 11c), the sail forces F_x and F_y are obviously at their maximum values (Fig. 9e, 9f). However, the leeward foil is almost entirely submerged (Fig. 11d) and is able to provide enough righting moment M_x (Fig. 9d) for the boat to maintain itself in the desired heeling angle range (Fig. 9a). This conjugation of limited heeling and maximal power coming from the sails, in addition to a bow-up position (Fig. 9b) which reduces the wetted area, allows the boat to sail at its optimal sailing speed. This contrasts with the Pogo sailing upwind test case (section 5.1), where a reduced sail power P_{ow} led to a better sailing speed V_B: when P_{ow} is reduced, in iterations 2 and 3 (Fig. 11a,11b), the sails do not provide enough power for the boat to heel and pitch as much, and the overall sailing speed decreases.

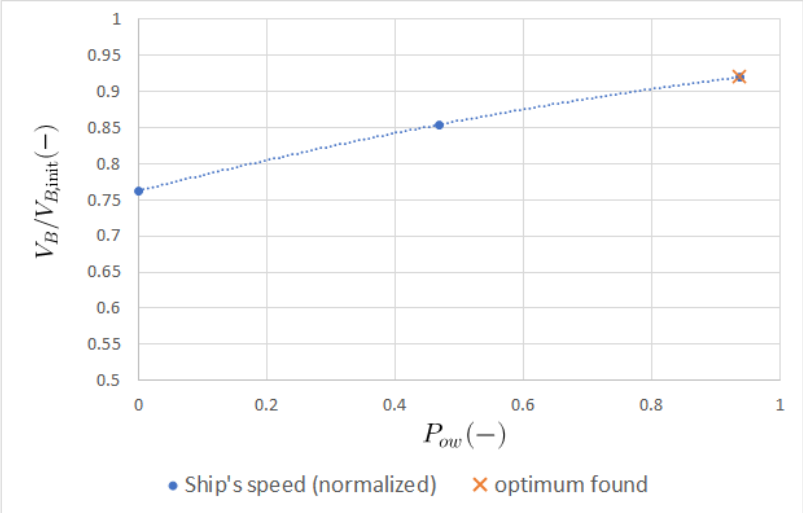

Figure 10. Sail power parameter optimisation for an IMOCA.

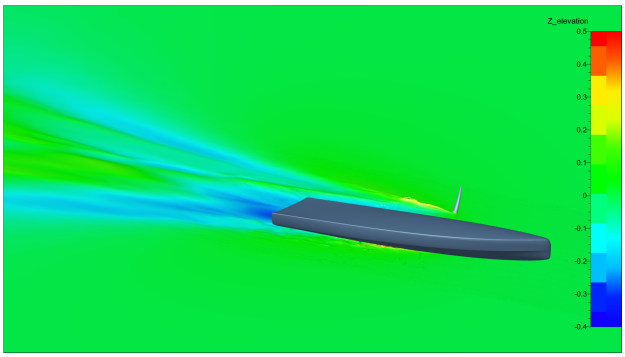

(a) Wavefield around the boat, $P_{ow} = 0$.

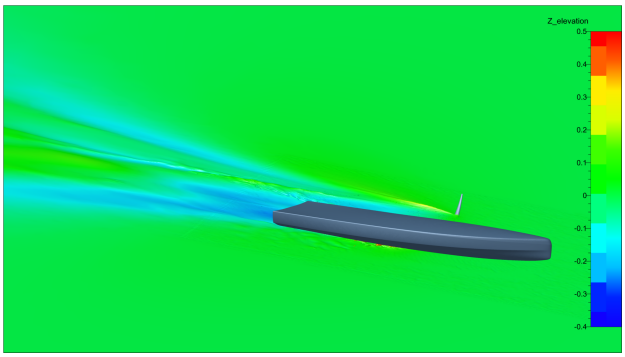

(b) Wavefield around the boat, $P_{ow} = 0.4683$.

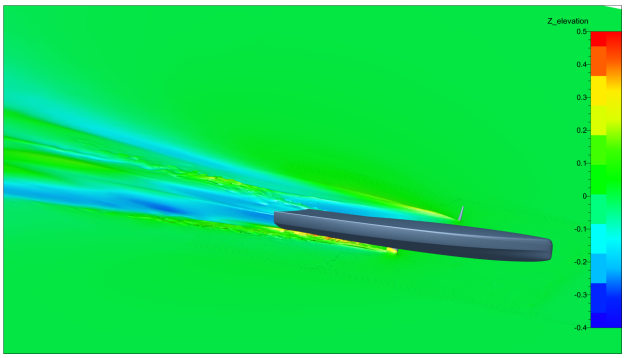

(c) Wavefield around the boat, $P_{ow} = 0.9367$.

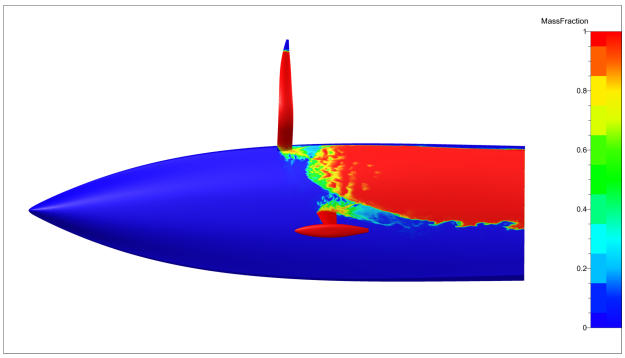

(d) Volume fraction, $P_{ow} = 0.9367$.

Figure 11. Results for an IMOCA 60' VPP simulation.

Since these yachts are recent and have confidential geometries, other VPP results or experimental data are not available. However, sea trials of the two real-life IMOCA show good agreement with the results obtained with our VPP.

6 DISCUSSION

The current VPP is part of a new paradigm for naval architects to assess their designs' performance. To compare it with other designs, a design can be correctly assessed with 5 to 10 carefully chosen operating points (β_t, V_a) which depend on the type of race the yacht is being designed for. This removes the need to construct full hydrodynamic matrices as required in a traditional static VPP.

An advantage of this approach is its speed. For sailing yachts without foils, a single operating point is typically calculated within half a day on a recent dual-AMD 7773X computer. In comparison, on the same machine, the 100+ computations required to build the hull's hydrodynamics matrix that feeds a static VPP, take over a week and require much more user time to setup and post-process. For racing yachts with foils, the computation time for the dynamic VPP is significantly longer, because of the larger number of cells required to capture the geometry of the foil with sufficient accuracy, and because of the occasional larger motions. Here, the computation time of the required operating points is comparable to that of the hull's hydrodynamic matrix.

A second advantage of our VPP lies in the accuracy of the method: the interactions between the hull and the appendages, and between the different appendages, are entirely taken into account as are the surface-piercing effects of the foils. Calculations have shown these interactions to be significant, especially for high-speed vessels with foils. Differences in leeway, for example, of up to 2° have been observed between our VPP and a static VPP with separate lifting line models for the appendages, which neglect these interactions.

However, the current approach is complementary to traditional VPPs and does not intend to replace them. Once a design is chosen, a traditional static VPP can supply a complete polar that can be used for a more global assessment of a design's performance, or for other applications such as weather routing or post-race performance analysis. Alternatively, VPP results (based on analytical formulas or CFD for hydrodynamics) can be calibrated using the high-fidelity results, as for the 40-feet fast cruiser presented in 5.1, where the VPP used seems to overpredict the yacht's speed when sailing upwind.

Being able to capture the behaviour of the yacht in waves is currently a major topic of development in ocean-going racing yachts. Thanks to the developments being implemented, the ability to carry out high fidelity 6-DoF dynamic simulation of a foiling boat in more realistic sailing conditions will be an added benefit to this VPP.

7 CONCLUSION

The aim of this work is to develop a VPP that will allow naval architects to perform high-fidelity studies of modern sailing boats using state-of-the-art CFD techniques. This paper showed through two yachts that such results can indeed be obtained. Moreover, in the scope of industrial use, this VPP program permits to perform high-fidelity studies for a few operating points of a design, in a way that is complementary to traditional VPPs.

Like many VPPs, the results obtained using this program would need comparison to experimental or real values to correctly obtain validation. In future works, authors hope to have access to real-life IMOCA yachts' race data and perform a comparison of the results obtained with the tool presented here to this data.

The authors are currently addressing several topics in order to enhance the different models and

the overall precision of the tool. One area for improvement lies within the FSI model, given that the modal approach does not consider non-linearities. Therefore, further works will compare this method to another approach where a coupling with a beam model structural solver is made. For the naval architect, the beam approach is interesting as it does not require the separate calculation step of the first deformation eigenmodes, and because the description of a foil as a beam, which is usually known, is directly input to the code.

It could also prove useful to be able to interpolate using more variables, an interpolation method based on radial-basis functions is thus being developed. For example, an interpolation based on P_{ow}, β_a, ϕ, V_a and a traveller position ω could be of interest. For such purposes, several radial-basis functions are available (Volpi et al., 2015), but based on our early results, the radial function $\varphi(r) = r^3$ appears to be an efficient choice to interpolate inside a sail plan's aerodynamic forces matrix, and is easy to implement.

The current aerodynamic model is quasi-static, and it is assumed that, when searching for equilibrium states, this limitation is acceptable. In the scope of future ship in waves simulations, an unsteady formulation is being studied.

REFERENCES

Böhm, C. (2014). A Velocity Prediction Procedure for Sailing Yachts with a Hydrodynamic Model Based on Integrated Fully Coupled RANSE-Free-Surface Simulations. PhD thesis. TU Delft.

Deng, G. B., Leroyer, A., Guilmineau, E., Queutey, P., Visonneau, M., Wackers, J., and Toro Llorens, A. del (2015). Verification and Validation of Resistance and Propulsion Computation. *Proceedings of Tokyo 2015 - A Workshop on Numerical Ship Hydrodynamics*. Tokyo.

Leroyer, A. (2021). Efficient and Robust FSI RANSE Simulations around Elongated Bodies for Hydrodynamic Applications, Minimally Intrusive for the Beam Solver. *Proceedings of MARINE 2021*. Online.

Leroyer, A. and Visonneau, M. (2005). Numerical Methods for RANSE Simulations of a Self-Propelled Fish-like Body. *Journal of Fluids and Structures* 20.7, pp. 975–991.

Lindstrand Levin, R. and Larsson, L. (2017). Sailing Yacht Performance Prediction Based on Coupled CFD and Rigid Body Dynamics in 6 Degrees of Freedom. *Ocean Engineering* 144, pp. 362–373.

Mouton, L., Leroyer, A., Deng, G. B., Queutey, P, Soler, T., and Ward, B. (2018). Towards Unsteady Approach for Future Flutter Calculation. *Journal of Sailing Technology* 3, pp. 1–19.

ORC, Offshore Racing Congress (2021). ORC VPP Documentation 2021. `https://www.orc.org/rules/ORC`.

Persson, A., Larsson, L., and Finnsgård, C. (2021). An Improved Procedure for Strongly Coupled Prediction of Sailing Yacht Performance. *Journal of Sailing Technology* 6.01, pp. 133–150.

Prince, M. and Claughton, A. (2016). The SYRF Wide Light Project. *Proceedings of SNAME 22nd Chesapeake Sailing Yacht Symposium*. Annapolis, Maryland, USA,

Pržulj, V. and Basara, B. (2001). Bounded convection schemes for unstructured grids. *15th AIAA Computational Fluid Dynamics Conference*. AIAA paper 2001-2593. Anaheim, CA.

Queutey, P. and Visonneau, M. (2007). An Interface Capturing Method for Free-Surface Hydrodynamic Flows. *Computers & Fluids* 36.9, pp. 1481–1510.

Robin, P., Leroyer, A., Richeux, J., Prémorel, D. de, and Wackers, J. (2022). Starting off the Right Foot with Foil Sock Approach and AGR criterion. *Proceedings of 24th Numerical Towing Tank Symposium.* Zagreb, Croatia.

Roux, Y., Durand, M., Leroyer, A., P., Queutey, Visonneau, M., Raymond, J., Finot, J-M., Hauville, F., and Purwanto, A. (2008). Strongly Coupled VPP and CFD RANSE Code for Sailing Yacht Performance Prediction. *Proceedings of 3rd High Performance Yacht Design Conference*. Auckland, New Zealand.

Volpi, S., Diez, M., Gaul, N., Song, H., Iemma, U., Choi, K., Campana, E., and Stern, F. (2015). Development and Validation of a Dynamic Metamodel Based on Stochastic Radial Basis Functions and Uncertainty Quantification. *Structural and Multidisciplinary Optimization* 51, pp. 347–368.

Waagmeest, J.P. (2023). *ORC Sailboat Data (2023)*. `https://jieter.github.io/orc-data/site/`.

Wackers, J., Deng, G. B., Guilmineau, E., Leroyer, A., Queutey, P., Visonneau, M., Palmieri, A., and A., Liverani (2017). Can Adaptive Grid Refinement Produce Grid-Independent Solutions for Incompressible Flows? *Journal of Computational Physics* 344, pp. 364–380.

Wackers, J., Deng, G.B., Raymond, C., Guilmineau, E., Leroyer, A., Queutey, P., and Visonneau, M. (2022). Adaptive Grid Refinement for Ship Resistance Computations. *Ocean Engineering* 250, p. 110969.

Wackers, J., Koren, B., Raven, H. C., Ploeg, A. van der, Starke, A.R., Deng, G. B., Queutey, P., Visonneau, M., Hino, T., and Ohashi, K. (2011). Free-surface Viscous Flow Solution Methods for Ship Hydrodynamics. *Archives of Computational Methods in Engineering* 18, pp. 1–41.